PROCEEDINGS, 43rd Workshop on Geothermal Reservoir Engineering
Stanford University, Stanford, California, February 12-14, 2018
SGP-TR-213

Predicting Hydraulic Fracture Trajectory Under the Influence of a Mine Drift in EGS Collab Experiment I

Pengcheng Fu[1], Mark D. White[2], Joseph P. Morris[1], Timothy J. Kneafsey[3], and EGS Collab Team[4]

[1] Atmospheric, Earth, and Energy Division, Lawrence Livermore National Laboratory, Livermore, CA 94526

[2] Pacific Northwest National Laboratory, Richland, WA 99352

[3] Lawrence Berkeley National Laboratory, Berkeley, CA 94720

Email: fu4@llnl.gov

Keywords: Hydraulic fracturing, enhanced geothermal system, EGS, SURF

ABSTRACT

Experiment I of the EGS Collab project entails drilling largely horizontal wellbores in phyllite of the Precambrian Poorman formation, at the Sanford Underground Research Facility (SURF), located at the former Homestake Gold Mine, in Lead, South Dakota, and creating/stimulating hydraulic fractures from one of the wellbores. The stimulation well was drilled from the old mine drift at the 4850 level (4850 feet deep from ground surface) along the minimum in situ principal stress direction and the fracture initiation point is approximately 40 m from the drift. An essential component of the experiment design is to predict the trajectory of the hydraulic fractures so that the production and monitoring wells can be drilled accordingly and precautionary measures can be taken to prevent the fracture from intersecting the drift. Through thermo-hydro-mechanical (THM) coupled simulation of the cooling and drainage history experienced by the drift, we calculate the temperature, pore pressure, and stress distributions around the drift. The calculated temperature is validated against measurements along existing vertical wells. The simulation results suggest that the cooling of the rock around the drift has caused very significant thermal stress with magnitudes up to several MPas near the fracture initiation point. The minimum principal stress decreases rapidly from this point toward the drift. A fully coupled hydraulic fracturing simulation indicates that the fracture would have a strong tendency to propagate toward the drift, driven by the radial gradient of the minimum principal stress. The fracture will remain planar until it curves and becomes parallel to the drift when the fracture front is a few meters from the drift. The role of these simulation results is twofold in the EGS Collab experiment: they guide experiment designs and will be used to validate the simulation codes against the actual experiment results.

1. INTRODUCTION

The EGS (enhanced geothermal system) Collab project, sponsored by the United States Department of Energy (DOE), Geothermal Technologies Office (GTO), focuses on intermediate-scale (~10-20 m) EGS reservoir creation processes and related model validation at crystalline rock sites. Three experiment sites will be developed to provide a collaborative experimental suite of field test beds coupled with stimulation and inter-well flow tests. After evaluating numerous potential project sites, the project team, lead by Lawrence Berkeley National Laboratory and comprised of multiple national laboratories and universities, selected the Sanford Underground Research Facility (SURF) in South Dakota as the first EGS Collab project site (Experiment I).

Current design of Experiment I, as schematically shown in Figure 1, includes drilling a number of largely horizontal wells, including a stimulation/injection well, a production (flow-back) well, and several monitoring wells, from the West Access Drift of SURF at 4850 ft (1478 m) blow ground in phyllite of Precambrian Poorman Formation. The orientations of the wells were based on in situ stress measurements made in the kISMET test (permeability (k), and Induced Seismicity Management for Energy Technologies; Oldenburg et al., 2016). The stimulation well is along the interpreted minimum principal stress (S_{hmin}) direction from kISMET, N4°W with a 12° down dip. Because the drift axis orients N33.5°E, the angle between the stimulation well axis and the drift axis is approximately 37.5° on a plan view. Multiple hydraulic fractures will be initiated at up to 60 m deep in the stimulation well, and they are expected to be perpendicular to the wellbore axis if the kISMET results prove accurate and the perturbation to the in situ stress from the drift proves to be minimal at

[4] J. Ajo-Franklin, S.J. Bauer, T. Baumgartner, K. Beckers, D. Blankenship, A. Bonneville, L. Boyd, S.T. Brown, J.A. Burghardt, T. Chen, Y. Chen, C. Condon, P.J. Cook, P.F. Dobson, T. Doe, C.A. Doughty, D. Elsworth, J. Feldman, A. Foris, L.P. Frash, Z. Frone, P. Fu, K. Gao, A. Ghassemi, H. Gudmundsdottir, Y. Guglielmi, G. Guthrie, B. Haimson, A. Hawkins, J. Heise, C.G. Herrick, M. Horn, R.N. Horne, J. Horner, M. Hu, H. Huang, L. Huang, K. Im, M. Ingraham, T.C. Johnson, B. Johnston, S. Karra, K. Kim, D.K. King, T. Kneafsey, H. Knox, J. Knox, D. Kumar, K. Kutun, M. Lee, K. Li, R. Lopez, M. Maceira, N. Makedonska, C. Marone, E. Mattson, M.W. McClure, J. McLennan, T. McLing, R.J. Mellors, E. Metcalfe, J. Miskimins, J.P. Morris, S. Nakagawa, G. Neupane, G. Newman, A. Nieto, C.M. Oldenburg, W. Pan, R. Pawar, P. Petrov, B. Pietzyk, R. Podgorney, Y. Polsky, S. Porse, S. Richard, M. Robertson, B. Roggenthen J. Rutqvist, H. Santos-Villalobos, P. Schwering, V. Sesetty, A. Singh, M.M. Smith, H. Sone, C.E. Strickland, J. Su, C. Ulrich, A. Vachaparampil ,C.A. Valladao, W. Vandermeer, G. Vandine, D. Vardiman, V.R.. Vermeul, J.L. Wagoner, H.F. Wang, J. Weers, J. White, M.D. White, P. Winterfeld, H. Wu, Y.S. Wu, Y. Wu, Y. Zhang, Y.Q. Zhang, J. Zhou, Q. Zhou, M.D. Zoback

the fracturing location. In the circulation experiment, this well will be used as the injection well; the production well, through which the circulation fluid returns, is largely parallel to the stimulation/injection well, with an approximately 10 m offset toward the drift direction. Several monitoring wells will be drilled from the drift, either parallel to the expected fracture plane or semi-parallel to the injection well, as illustrated in Figure 1. Multiple geophysical methods including continuous active-source seismic monitoring (CASSM), microseismic (MEQ), electrical resistivity tomography (ERT), and continuous distributed monitoring of temperature, seismicity, and strain using fiber optic cable will be performed in these observation wells (Knox et al. 2017). The present work evaluates the influence of the mine drift, through the following two mechanisms, on the predicted hydraulic fracture trajectory as well as the impacts on the experiment design:

1. The concentration and redistribution of in situ stress around the drift caused by the stress-free condition on the drift surface; and
2. The drift's alteration of the temperature and pore pressure fields by the drainage and ventilation history.

These factors could influence a series of design and operation decisions regarding the location of stimulation (i.e. depth along the wellbore), expected pumping power, measures to prevent the fracture intersecting the drift, etc. We use coupled thermo-hydro-mechanical (THM) simulation to address these issues.

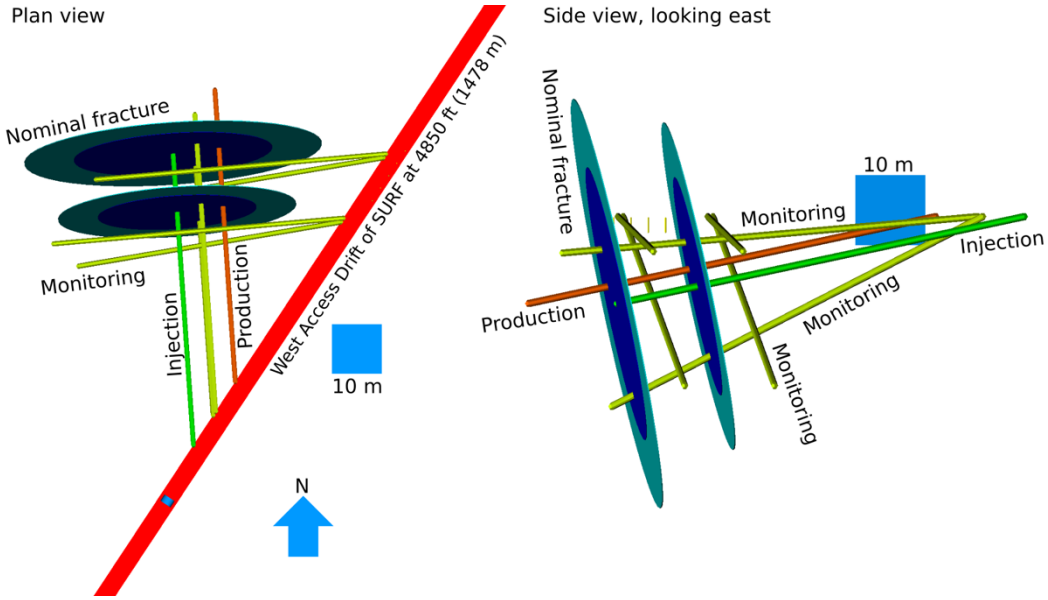

Figure 1 Layout of the planned wellbores and their intended functions. The floor of the drift is shown in the plan view. Two nominal penny-shaped fractures are shown to indicate the spatial relationship between them and the wells. A cube, 10 m long in each dimension is placed in the plots to provide a scale.

2. THE EFFECTS OF THE DRIFT ON THE SURROUNDING TEMPERATURE AND PORE PRESSURE FIELDS

A series of numerical simulations were executed, with STOMP-GT (White and Oostrom, 2006), to determine the temperature, pore pressure, and fluid saturation profiles around the 4850 Level West Access Drift at SURF. These profiles were controlled by the ambient geothermal gradient, hydrological state and the historical mining operations. Temperature measurements taken during the underground reconnaissance for the DUSEL facility (Dobson and Salve, 2009) and during the EGS-Collab project within the kISMET boreholes (Oldenburg et al., 2016; Roggenthen and King, 2017) were used for verification of the numerical simulation results. The 4850 Level West Access Drift at SURF was excavated during the mining activities of the Homestake Gold Mine, which began in the late 1870s and continued until 2001, with cessation of mine production. Dewatering of the mine continued for two years, but on June 10, 2003 the pumps were switched off and the mine closed. The Homestake mine workings advanced in depth and lateral spread over time in a complex pattern, driven by the search for higher-grade ore bodies, but the overall depth of the mine increased at a fairly uniform rate of 26 m/yr (Murdoch et al., 2012). Assuming that the water level in the mine followed the progression of the mine workings, drifting of the 4850 Level started in early 1949 (Murdoch et al., 2012). Anderson (1983) modeled temperature profiles around the 8000 Level drift, with a two-dimensional finite-element model. Following cessation of mining operations in 2001 and then active dewatering in 2003, the water level in the mine increased from steadily at a rate of 0.56 m/day (Davis et al., 2009), with the water level reaching the 8000 Level on June 17, 2003. Extrapolating the Davis et al. (2009) data to the 4850 Level, yielded a flooding date of September 1, 2007. Table 1 documents the chronological events associated with modeling the profiles around 4850 Level West Access Drift at SURF.

Table 1. 4850 Level Modeling Events Chronology

Days	Date	Event	Drift-Wall Boundary Conditions
0	3/3/1949	4850 Level Drifting Starts	Advective, 26.0˚C, 5.0 W/m^2 K
19,829	6/17/2003	Homestake Mine Closed	Adiabatic, Zero Flux
21,366	9/1/2007	4850 Level Flooded	Adiabatic, Zero Flux
21,986	5/13/2009	4850 Level Dewatered	Evaporative, 26.0-20.2˚C, 1.5 m/s, 0.85 RH, 5.0 W/m^2 K
22,014	6/10/2009	4850 Level LBNL Survey Start	Evaporative, 26.0-20.2˚C, 1.5 m/s, 0.85 RH, 5.0 W/m^2 K
22,061	6/10/2009	4850 Level LBNL Survey End	Evaporative, 26.0-20.2˚C, 1.5 m/s, 0.85 RH, 5.0 W/m^2 K
24,904	5/9/2017	4850 Level kISMET Survey	

The conceptual model for the numerical simulations was that the phyllite rock surrounding the 4580 Level West Access Drift was homogeneous with constant intrinsic properties and void of hydraulically conductive fractures. Simulations were executed on a structured boundary fitted 2-dimensional domain that extended horizontally 100 m from the drift center line, and 100 m vertically in both directions from the drift midheight. The outer lateral boundary condition was set to be hydrostatic with a geothermal gradient, with a reference pressure of 14.674 MPa at a depth of 1576.48 m, and a reference temperature of 36.42˚C, at a reference depth of 1572.76 m, with a geothermal gradient of 0.02097 ˚C/m (i.e., increasing with depth). The boundary condition on the drift wall, ceiling, and floor varied with time, as shown in Table 1. During the period from 1949 through the mine closure in 2003, an advective boundary condition was applied with a constant air temperature of 26 ˚C, and an overall heat transfer coefficient of 5.0 W/m^2 K. The advective boundary condition did not consider drying of the rock adjacent to the drift. During the period between mine closure and dewatering of the 4850 Level, an adiabatic, zero flux boundary condition was applied. This boundary condition ignores heat transfer and fluid flow between the phyllite and drift, and does not consider the heat capacitance of air and water in the drift. At the point of dewatering it was assumed that the rock was saturated. An evaporative boundary condition was then applied with a drift air temperature that decreased from 24˚C to 20.2˚C between 2009 and 2017, an air velocity of 1.5 m/s, and an air relative humidity of 85%. An advective heat transfer coefficient of 5.0 W/m^2 K was additionally applied. Simulations were initialized with an aqueous saturation of 1.0, with a pressure of 14.637 MPa at a depth of 1572.76 m and pressure gradient of 0.0098 MPa/m (i.e., increasing with depth), and a temperature of 36.42˚C, at a reference depth of 1572.76 m, with a geothermal gradient of 0.02097 ˚C/m (i.e., increasing with depth). Petrophysical properties of the phyllite used in the numerical simulation are listed in Table 2. Values for grain density, and grain specific heat were equivalent to those used by Ashworth (1983) in the numerical simulations of the 8000 Level drift. Thermal conductivity and intrinsic permeability were determined from 1-dimensional simulations of drift cooling with evaporation, compared against the kISMET measurements of Roggenthen (2017). Ashworth (1983) determined a thermal conductivity of 3.6 W/m K from laboratory measurements, lower than the value of 5.0 W/m K, used in this study. The capillary pressure versus saturation function was the van Genuchten (1980) model with a Webb extension (Webb, 2000), and the aqueous and gas relative permeabilities were computed from the Mualem model.

Table 2. 4850 Level Phyllite Petrophysical Properties

Property	Value	Property	Value	Property	Value
Grain Density	2900 kg/m^3	Intrinsic Permeability	5.0 x 10^{-18} m^2	van Genuchten m	0.346
Porosity	0.01	Thermal Conductivity	5.0 W/m K	Residual Saturation	0.06
Pore Compressibility	7.2 x 10^{-16} 1/Pa	van Genuchten α	0.186 1/m	Ovendry Head	1.0 x 10^5 m
Grain Specific Heat	805 J/kg K	van Genuchten n	1.529		

Two series of temperature measurements served as verification marks for the numerical simulations. Shortly after dewatering of the 4850 Level, Dobson and Salve (2009) made measurements of the temperature of the phyllite rock in a new horizontal borehole drilled to a depth of approximately 2.4 m (i.e., 3.2 m from the drift centerline) and air temperature measurements. The temperature in the borehole showed a decay from 28.58˚C to 26.90˚C over a period of 47 days. These measurements provided a verification of evaporative cooling rates. At the start of the EGS Collab project Roggenthen (2017) made a series of measurements in the near veritical kISMET #3 (Oldenburg et al., 2016) borehole. These measurements provided a verification of the current temperature profile around the 4850 Level drift. The temperature and aqueous saturation profiles for 05/09/2017, the time of the kISMET measurements (Roggenthen, 2017), is shown in Figure 2. The temperature profile shows both the impact of the long-term drift cooling which occurred from 1949 through 2003, and then

the more recent higher-rate evaporative cooling from 2009 through 2017. The impact of evaporative cooling is time limited, as thin dryout region develops around the drift wall, reducing relative permeability of the rock and evaporation rate.

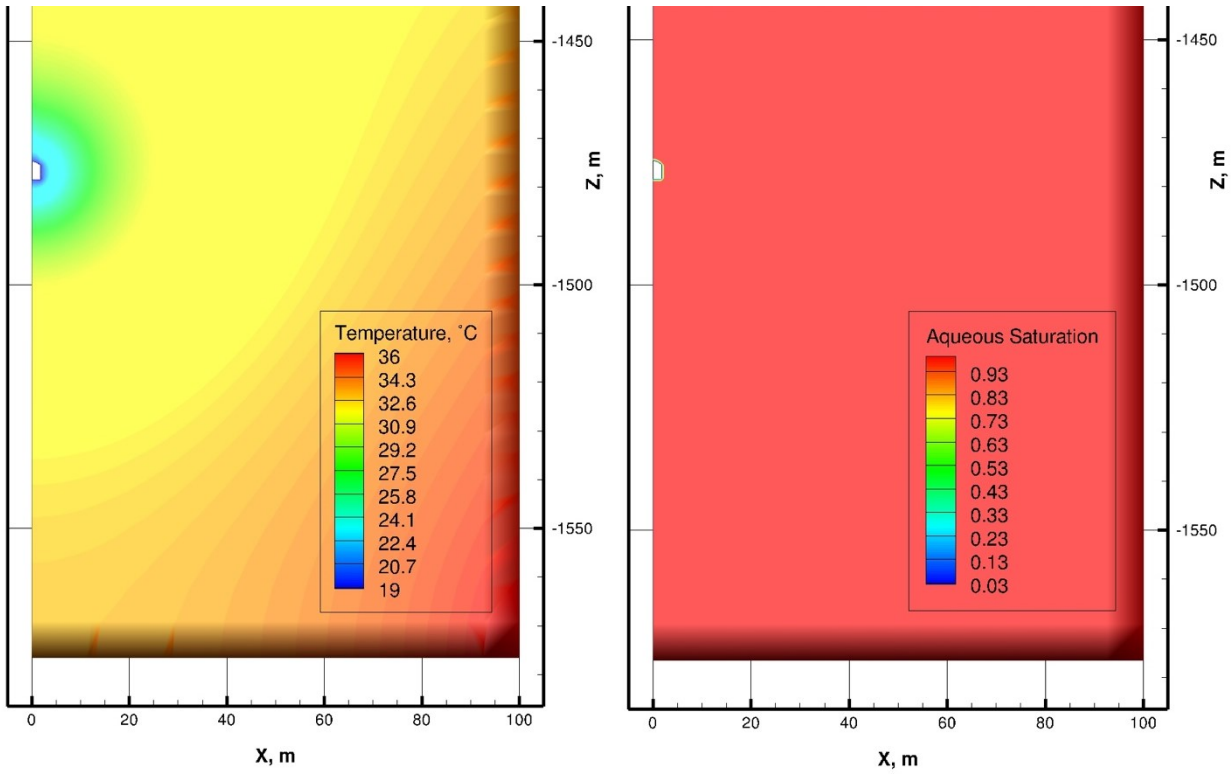

Figure 2 Numerical simulations of temperature and aqueous saturation profiles around 4850 Level drift at 05/09/2017.

Linear temperature profiles at six points in time along a horizontal line from the drift wall to the outer later boundary, reference from the drift centerline, are shown in Figure 3. The initial condition is set at the start of 4850 Level drifting at 03/03/1949. At the time of mine closure on 06/17/2003, the impact of advective cooling can be seen, reducing the temperatures in a radial pattern around the drift. During the mine closure, the adiabatic, zero-flux boundary conditions on the drift wall, yielded recover of the temperature profile, with the drift wall reaching approximately 32˚C. With dewatering of the 4850 Level, evaporative cooling resulted in a rapid decline in the near drift temperature, and the numerical simulations show good agreement with the measurements, both in terms of magnitude and change over the 47-day period, taken during the LBNL survey (Dobson and Salve, 2009). Linear temperature profiles at six points in time along a vertical line from the drift floor to the lower horizontal boundary, reference from the mine surface, are shown in Figure 4. Similar trends in the temperature profiles over time are observed in these plots as the system is generally dominated by radial heat transport and fluid flow. The kISMET #3 borehole measurements (Roggenthen, 2017) are shown as makers on the plot. The numerical simulation results at 05/09/2017 show similar profiles, with a slight offset. Whereas, the LBNL survey (Dobson and Salve, 2009) measurements are a strong indicator of evaporation rates, the kISMET survey (Roggenthen, 2017) provides an indication of the total history of the 4850 Level, for which there is little information about conditions within the drift. The objective of this numerical study was to develop temperature profiles around the 4850 Level West Access Drift that could be used as initial conditions for future thermal circulation experiments, but also in support of the fracture stimulation activities, associated with Experiment 1. Temperatures obtained from the two surveys provided verification marks for defining simulation parameters and setting early-time boundary condition values for the drift. Optimization simulations could be executed to yield improved parameter fits, but would not greatly alter the resulting temperature profiles.

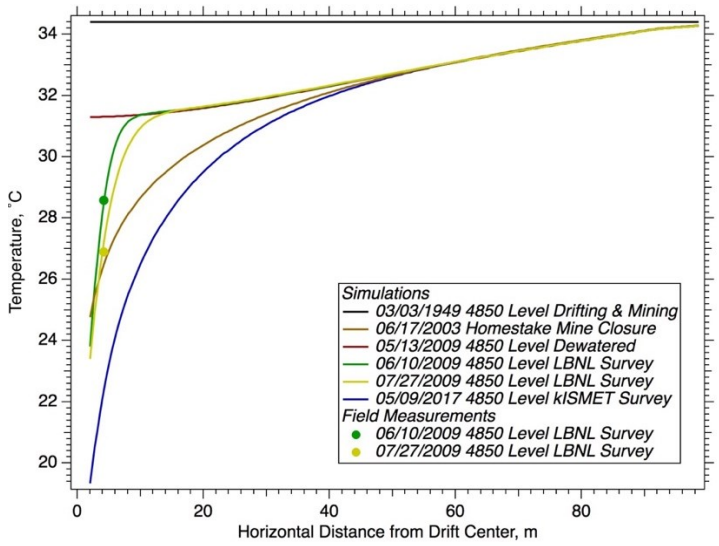

Figure 3 Temperature profiles along a horizontal line from the 4850 Level drift wall (referenced from the drift centerline).

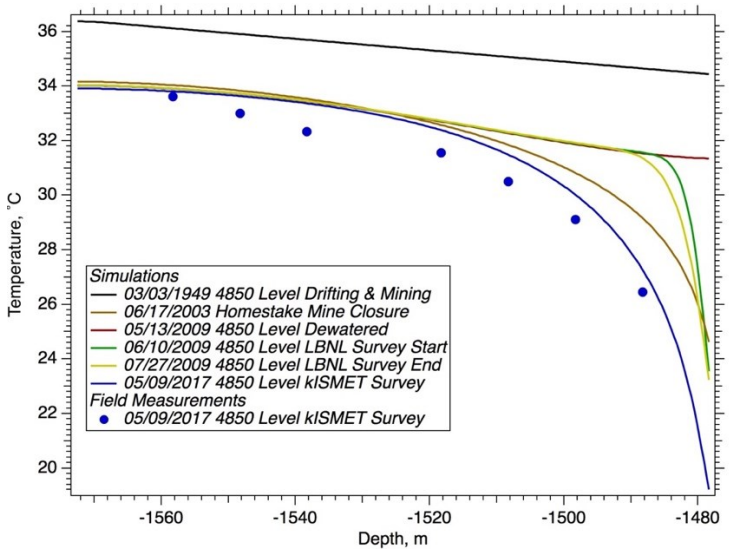

Figure 4 Temperature profiles along a vertical line from the 4850 Level drift floor (referenced from the mine surface).

3. STRESS PERTURBATION CAUSED BY THE DRIFT

3.1 Stress Analysis Model Setup

The alteration to the temperature and pore pressure calculated above is expected to perturb the stress field around the drift. Additionally, the stress-free condition on the drift wall also has some effect on the surrounding stress field.

A pore pressure change can alter the stress state (both total stress and effective stress) through the poroelastic effect. The relationship between the total stress tensor $\boldsymbol{\sigma}$, the effective stress tensor $\boldsymbol{\sigma}'$, and the pore pressure P_p is embodied by the principle of effective stress

$$\boldsymbol{\sigma} = \boldsymbol{\sigma}' - bP_p\mathbf{I}$$

$$b = 1 - \frac{K_{dr}}{K_s}$$

where b is the Biot coefficient that quantifies the intensity of the coupling between pore pressure change and stress change, K_{dr} is the drained bulk modulus of the porous medium, and K_s is the bulk modulus of the solid grain constituting the solid skeleton of the porous medium. Note that when presenting stress measurement results, we adopt the geomechanics sign convention where compression is positive. We adopt the solid mechanics sign convention, with tensile stress being positive, when presenting mathematical formulations. The phyllite at the experiment site is observed to be very dense, with small porosity, small permeability, and great stiffness. Since $K_{dr} \approx K_s$

and thereby $b \approx 1.0$, the pore pressure change is expected to only have minimal effects on the stress state in the rock formation. Moreover, in low permeability rocks, hydraulic fractures open against total normal stress rather than the effective normal stress. Therefore, all subsequent analyses are based on total stresses and do not explicitly deal with the pore pressure.

We build a solid finite element model in GEOS (Settgast et al., 2017) to evaluate the stress field near the drift. We use a rectilinear mesh with its y-axis along the drift axis (N33.5°E). The mesh is 200 m wide (100 m to both sides of the drift), 300 m long along the drift direction, and extends 100 m above and below the drift. The mesh resolution is 0.45 m near the drift and the element size progressively becomes larger toward the boundaries. The model includes approximately 4.3 million hexahedral elements.

We first initialize the stress state of the simulation domain with the best estimate from the kISMET, which indicated that near the drift depth, S_{hmin} = 21.7 MPa, striking N4°W with a 12° dip, S_{hmax} = 35.5 MPa, and S_v = 41.8 MPa. Note that the "vertical" stress S_v slightly deviates from vertical according to the measurements. The stress tensor (complying with solid mechanics sign convention) in the mesh coordinate system at the drift depth is

$$\boldsymbol{\sigma} = \begin{bmatrix} -30.708 & -6.245 & 2.488 \\ -6.245 & -27.361 & -3.243 \\ 2.488 & -3.243 & -40.931 \end{bmatrix} \text{MPa}$$

We assume that each stress component has a linear vertical gradient with zero value at the ground surface. The initial reference temperature field is corresponding to the ambient geothermal gradient described in section 2. Subsequently, we remove the solid elements inside the drift (3.6 m wide, 3.6 high, with an idealized arc roof) and impose the temperature field obtained in the previous section to calculate the altered stress field (Guo et al., 2016) due to both the mechanical cavity and the temperature perturbation.

3.2 Implications of the Stress Perturbation for Fracture Initiation

In this section, we investigate the effects of the stress perturbation caused by the drift on the expected fracture initiation modes in the wellbores. We consider two wellbores with idealized geometries: a stimulation well along N4°W and a monitoring well along N94°W, both drilled from the northwest wall of the drift at mid-height. Note that to facilitate stress conversion, we ignore the minor dipping of the actual wells. The cross-sections of these two wellbores are subjected to different configurations of stresses as shown in Figure 5. In either case, fluid pressurization in the wellbore could cause concentration of the hoop stress and eventually the initiation of a vertical axial fracture from the top or bottom of the wellbore. According to the Kirsch equations, the pressure required to initiate an axial fracture is $3S_{Hmax}$-S_v+S_t for the stimulation well and $3S_{hmin}$-S_v+S_t for the observation well, where S_t (≈2 MPa) is the tensile strength of the rock. We query the stress tensor along the two wells in the finite element model and plot several components concerned in the design in Figure 6. Note that stress components reflect the perturbation caused by the drift but not the stress concentration caused by the wellbore. However, the wellbore-induced stress concentration is reflected by the estimated pressure required to initiate an axial fracture.

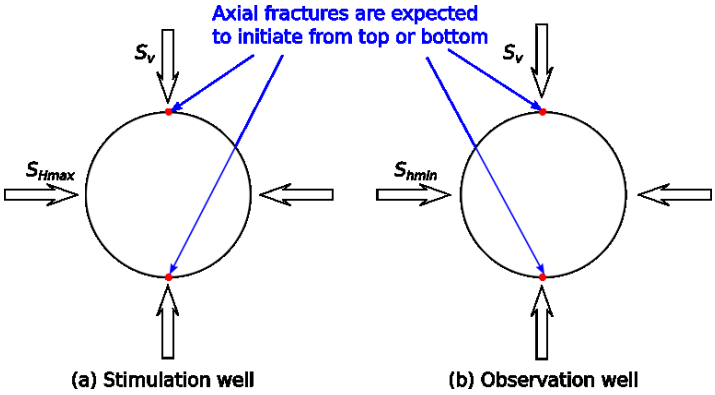

Figure 5 Loading Scenarios and expected fracture initiation patterns for an idealized stimulation well and an idealized observation well.

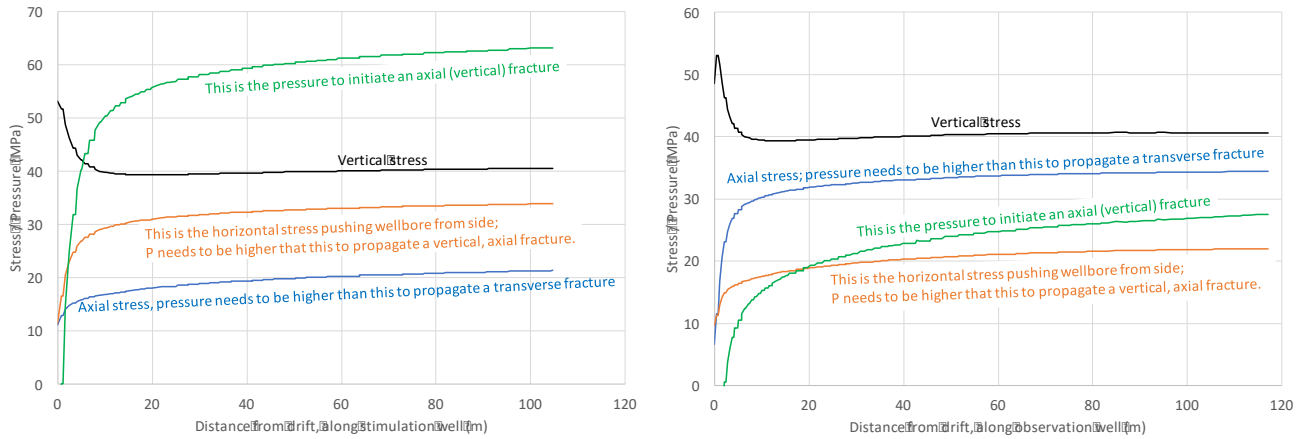

Figure 6 Stress distribution along an idealized stimulation well (left) and an idealized observation well (right). The stress perturbation caused by the drift, including the thermal effects is included. The stress distributions are those along the well locations without the presence of the wellbores themselves. Wellbore stress concentration is considered in calculating the pressure required to initiate an axial fracture (green curves).

The stress query results in Figure 6 indicate that:

1. The drift has perturbed the stress field substantially in the first 6 m of either wellbore. In this region, the dominant mechanism is the stress-free condition on the drift walls. In deeper locations along either well, the temperature gradient caused by the drift generates a relatively gentle stress gradient. Generally, higher pressure is required to initiate and propagate a hydraulic fracture in deeper locations.

2. Along the stimulation well, the pressure required to propagate a transverse fracture (perpendicular to S_{hmin}) is much lower than that required to initiate and propagate an axial fracture. Note that the pressure required to initiate a transverse fracture (the breakdown pressure) heavily depends on the perforation or notching mechanism adopted, and is beyond the scope of the current work.

3. Along the observation well, the pressure required to initiate and propagate an axial fracture is significantly lower than the pressure that drives a transverse fracture. Therefore, transverse fracture is an unlikely scenario for this well.

3.3 Implications of the Stress Perturbation for Fracture Propagation

A hydraulic fracture tends to propagate perpendicular to the minimum principal stress direction (King and Willis, 1957) and also tends to propagate toward regions with lower stresses. Since the majority of the energy input in a hydraulic stimulation is used to overcome the compressive stress acting on the fracture plane, the most important mechanism through which the drift affects the fracture propagation is its influence on the minimum principal stress. Figure 7 shows the temperature field (a) and the magnitude of minimum principal stress (b) along the expected fracture plane (N94°W, 78° dipping). The results show that the temperature perturbation caused by the drainage and ventilation history of the drift has reached the planned fracturing location and so has the corresponding stress alteration.

Figure 8 quantifies the temperature and stress perturbation by plotting these two quantities along a horizontal query line along the expected fracture plane at mid-height of the drift. If the transverse fracture is to be initiated at 60 m deep in the stimulation well, the initiation point is approximately 50 m from the drift axis along the fracture plane, as labeled in Figure 8. The horizontal gradient of S_{hmin} at this location is approximately 40 kPa/m, more than four times the hydrostatic gradient. Consequently, the hydraulic fracture is expected to have a strong tendency to propagate toward the drift, which will be verified using a fully coupled hydraulic fracturing model in the next section. The results also suggest that the presence of the drift reduces the pressure required to propagate a hydraulic fracture at this location by one to two MPa. This reduction would become much more significant if the hydraulic fracture is to be initiated closer to the drift (shallower along the stimulation well), but its tendency to propagate toward the drift and the associated risk of intersecting the drift would also become greater.

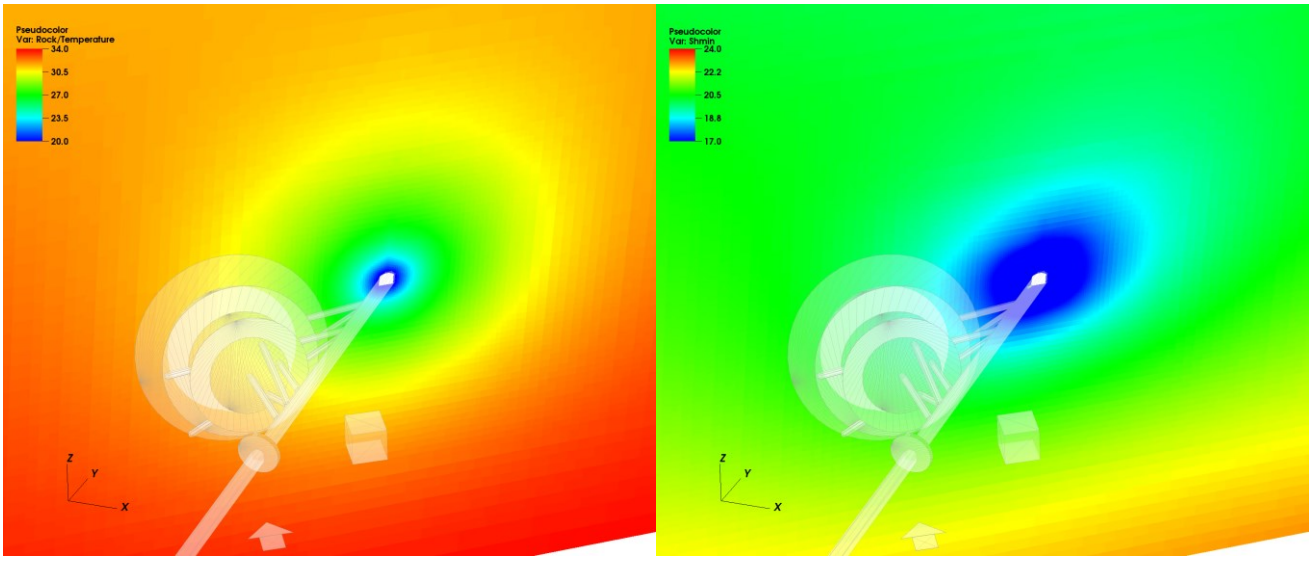

(a) (b)

Figure 7 The (a) temperature and (b) stress (minimum principal stress) perturbations caused by the drift along the expected fracture plane. The profiles of the drift, the planned wells, and the hypothetical fractures are shown in semi-transparency.

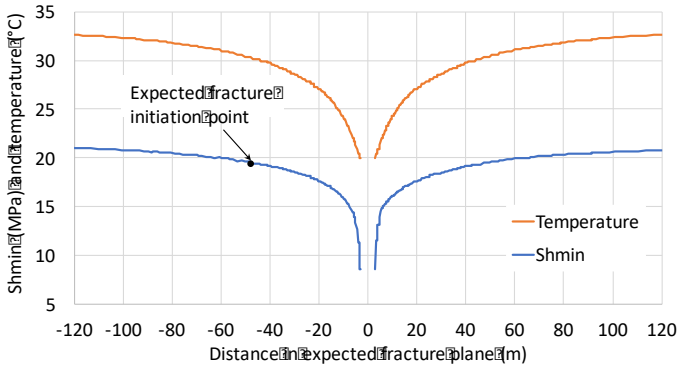

Figure 8 The temperature and minimum principal stress distributions along a horizontal line within the expected fracture plane at mid-height of the drift. The expected fracture initiation point is marked, where the horizontal gradient of S_{hmin} is approximately 40 kPa/m.

4. HYDRAULIC FRACTURING SIMULATION UNDER THE PERTURBED STRESS

In this section, we simulate the propagation of a hydraulic fracture under the stress perturbation calculated in section 3. We employ a fully coupled hydraulic fracture simulation code, GEOS, developed at the Lawrence Livermore National Laboratory (Fu et al., 2013; Settgast et al., 2017) as the primary tool for this purpose. To simulate hydraulic fracturing, GEOS couples a finite element method (FEM) for mechanical response of the solid matrix, a finite volume method (FVM) based on lubrication theory for the fluid flow along fractures, and the linear elastic fracture mechanics (LEFM) for the fracturing criterion. FVM is also used in GEOS to model porous medium flow in the rock matrix, but that module is not invoked in the current study as matrix flow does not play a significant role in the phenomena being studied. New fracture area is generated by duplicating the "face element" connecting two adjacent solid elements in the original continuum body. New face flow elements are thereby added to the fracture slow system. The FEM and FVM are naturally coupled: the fluid pressure from the flow module is applied to the surface of the fracture in the solid mesh, while the solid deformation determines the aperture (which in turn determines hydraulic impedance and storage) of the fracture. Momentum balance is satisfied at each time step on the current updated mesh topology whereas fluid mass conservation is satisfied across the fracture flow system. The formulation of GEOS's hydraulic fracturing module as well as extensive verification and validation studies has been reported in Settgast et al. (2017).

The mesh for the hydraulic fracturing simulation is different from that for the thermal stress calculation in a number of ways. To make the simulation computationally tractable, the mesh has a lower resolution, 0.9 m near the drift and around the expected hydraulic fracturing trajectory. We use prism elements to generate grid lines/planes complying with the drift boundaries and the expected fracture plane. Approximately 1.7 million prism elements are used in the simulation. The same mechanical and thermal boundary conditions as those for the thermal stress analysis are applied to the hydraulic fracturing model. The injection point (where the hydraulic fracture is

initiated) is 38.4 m to the left of and 14.0 m below the axis of the drift. The distance between the injection point and the drift axis is approximately 51 m along the expected fracture plane. Water with a nominal viscosity of 1.0 cP is injected at a rate of 0.1 L/s, which is in the higher end of the planned stimulation rate. The critical stress intensity factor (K_{IC}, commonly known as the "toughness" of the rock) is assumed to be 1.0 MPa·m$^{0.5}$.

The simulated fracture shape and aperture distribution after 6 minutes of stimulation are shown in Figure 9. Shown in the background is the magnitude of the minimum principal stress in the rock body on a planar "slice" that is parallel to and 5 m away from the expected fracture plane. Instead of forming a "penny" shape around the stimulation well as the initial experiment design had envisioned, the fracture shows a very strong tendency to grow toward the drift, driven by the great gradient of S_{hmin}. As shown in Figure 8, the gradient is approximately 40 kPa/m at the fracture initiation point and increases as the fracture approaches the drift. The aperture near the injection point (0.15 mm) is close to the value estimated based on a toughness-dominated penny-shaped hydraulic fracture. The aperture is smaller at locations farther from the injection but could be larger when the fracture is near the drift, due to the very low local stresses.

We have to caution the readers for two potential artifacts in the simulation results. The S_{hmin} gradient, or more strictly speaking, the difference between the S_{hmin} gradient and the hydrostatic pressure gradient, which drives the propagation of the hydraulic fracture, points toward the drift. The hydraulic fracture is expected to propagate directly toward the drift too. In the simulation results, however, the fracture first grows towards the drift but along a largely horizontal direction before it turns directly toward the drift when the fracture front is approximately 20 m away from the drift. This is believed to be an artifact caused by the combination of some imperfection in the fracturing criterion and the structure in the mesh. In other words, we believe that the fracture should propagate directly toward the drift instead of moving horizontally before turning toward the drift as shown in the simulation results. The second potential artifact is that when the fracture propagates to very close to the drift, it may deviate from the largely planar trajectory and "turn" due to the remarkable rotation of principal in situ stress near the drift. Since in GEOS the fracture can only propagate along existing mesh faces, the turning might be restricted by the adopted mesh configuration. We analyze the potential turning of the fracture in next section.

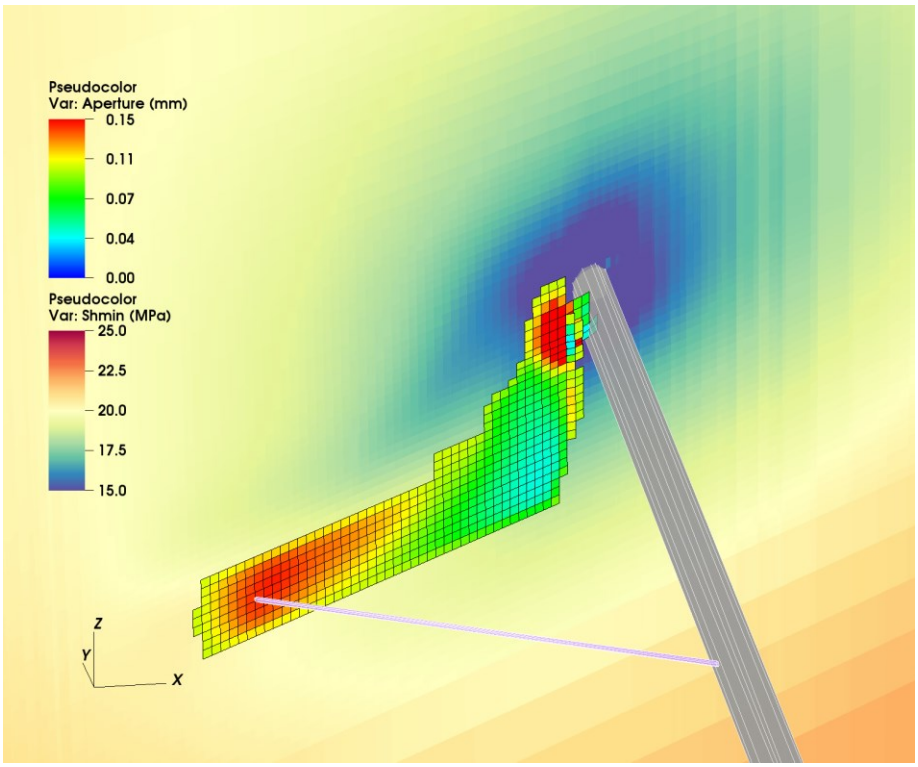

Figure 9 Fracture extents and aperture distribution after 6 minutes of injection at 0.1 L/s under the strong influence of the stress perturbation caused by the drift. Shown in the background is the magnitude of the minimum principal stress in the rock body on a planar "slice" that is parallel to and 5 m away from the expected fracture plane. The locations of the drift and the planned stimulation well are shown in the figure.

5. HYDRAULIC FRACTURING TURNING NEAR DRIFT

Since a reliable numerical model that allows a hydraulic fracture to turn freely without being constrained by the background mesh is not available, we perform a simplified trajectory analysis based on the orientations of the perturbed stress. Based on the modeling results in section 3, the orientations of S_{hmin} and S_{Hmax}, which are by definition perpendicular to each other, on a horizontal "slice" cutting the drift at mid-height are plotted in Figure 10. The magnitude of S_{hmin} decreases and its direction becomes more perpendicular to the drift wall at locations closer to the drift. The magnitude of S_{hmin} actually diminishes to zero at the drift wall due to the zero-stress boundary condition.

The magnitude of S_{Hmax} also decreases to a finite value and becomes parallel to the drift. We assume the hydraulic fracture remains to be perpendicular to the local S_{hmin} direction, which is likely to be valid for the expected experiment condition where the aperture is small and stress perturbation caused by the fluid pressure in the fracture is minimal. We predict the curved trajectory of the fracture to approximately follow the dashed line denoted in Figure 10, which eventually becomes parallel to the drift wall. The turning or the deviation from the original fracture plane is only significant when distance between the fracture front and the drift wall is close to or less than the width of the drift. Note that this visualization of stress rotation is at the mid-height of the drift. Near the floor and roof the drift, the minimum principal stress also becomes perpendicular to the floor and the roof, respectively. Therefore, the fracture could turn to become parallel to the roof and floor too at these locations.

It has been shown both experimentally and numerically that a hydraulic fracture originally propagating parallel to a free surface could turn toward the surface, thereby "daylighting" at the surface (Bunger, 2005). According to Bunger (2005), the daylighting radius can be predicted with $R = 4.4\chi + 3.2$, where $\chi = \sigma_r H^{0.5}/K_{IC}$, σ_r is the stress parallel to the free surface, and H is the distance to the free surface. Near the drift, σ_r=S_{Hmax}≈15 MPa, so even when the fracture is only 1.0 m from the drift wall, the daylight radius is 70 m, indicating rather weak tendency of the fracture turn toward the drift.

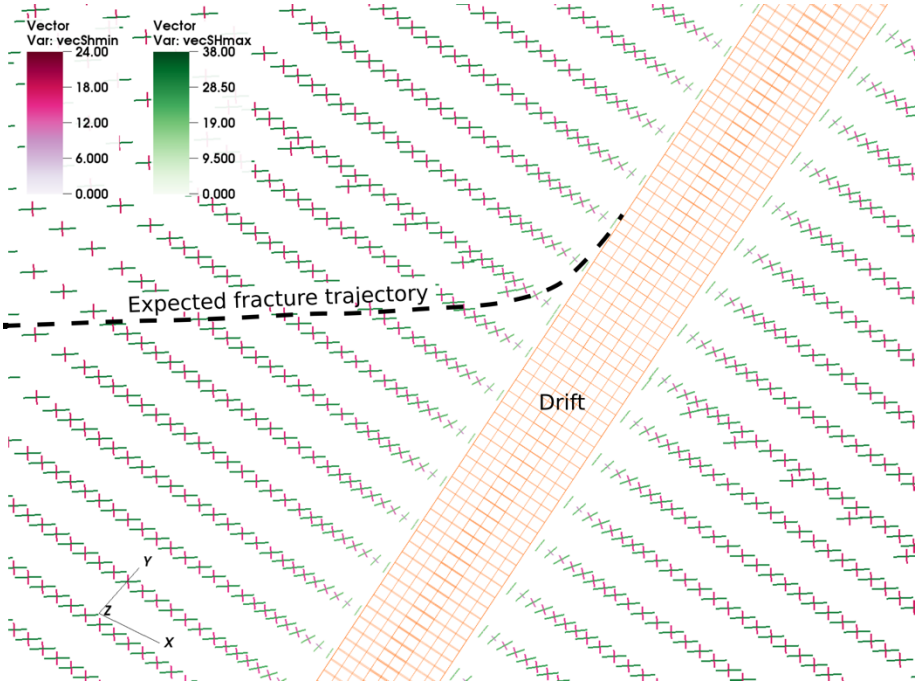

Figure 10 Prediction of fracture trajectory (and curving) if the hydraulic fracture is assumed to remain perpendicular to the local minimum principal stress direction. The short green lines represent the direction and magnitude of S_{hmin} and the short purple lines present S_{Hmax} on a horizontal "slice" cutting through the model at mid-height of the drift.

6. CONCLUSIONS AND IMPLICATIONS FOR EXPERIMENT DESIGN

We studied the perturbations caused by the SURF West Access Drift to the temperature and stress fields in the surrounding rock and the influence on the EGS Collab Experiment I that will be performed near the drift. The following conclusions are directly related to the design and execution of the experiment and interpretation of the experiment results.

1. The perturbations are caused by the stress-free condition on drift walls, as well as drainage and ventilation histories in the drift. The stress perturbation induced by the first mechanism is strong in the first several meters of rock around the drift and vanishes quickly at farther distances. The effects of drainage and ventilation reaches tens of meters into the rock, directly affecting the rock body where the hydraulic fracture will be initiated and propagate in.
2. The thermal contraction causes more than 5 MPa of reduction in minimum principal stress (S_{hmin}) near the drift. At the expected location for fracture initiation, the reduction is approximately 2 MPa.
3. The horizontal gradient of S_{hmin} at the fracture initiation point is approximately 40 kPa/m and the gradient increases as the fracture front propagates closer to the drift. This gradient is expected to drive the hydraulic fracture toward the drift, as confirmed by a fully coupled hydraulic fracturing model.
4. A simple stress rotation-based analysis predicts that the hydraulic fracture will show a tendency to curve and become parallel to the drift surface when the fracture front is within 2 meters of the drift wall. The tendency of the fracture to intersect the drift surface and "daylight" itself is weak due to the high compressive stress along the drift axis direction.

ACKNOWLEDGMENTS:

This material was based upon work supported by the U.S. Department of Energy, Office of Energy Efficiency and Renewable Energy (EERE), Office of Technology Development, Geothermal Technologies Program, under Award Number DE-AC52-07NA27344 with

LLNL, Award Number DE-AC05-76RL01830 with PNNL, and Award Number DE-AC02-05CH11231 with LBNL. Publication releases for this manuscript are under LLNL-CONF-744562and PNNL-SA-131598. The United States Government retains, and the publisher, by accepting the article for publication, acknowledges that the United States Government retains a non-exclusive, paid-up, irrevocable, world-wide license to publish or reproduce the published form of this manuscript, or allow others to do so, for United States Government purposes. The research supporting this work took place in whole or in part at the Sanford Underground Research Facility in Lead, South Dakota. The assistance of the Sanford Underground Research Facility and its personnel in providing physical access and general logistical and technical support is acknowledged.

REFERENCES

Ashworth, E.: The applications of finite element analysis to thermal conductivity measurements, *Master of Science Thesis*, South Dakota School of Mines and Technology, Rapid City, South Dakota (1983).

Bunger, A.P.: *Near-Surface Hydraulic Fracture*, (2005), doctoral dissertation, University of Minnesota, Minneapolis, MN.

Davis, A.D., L.D. Stetler, W.M. Roggenthen, Z.J. Hladysz, and R. Salve.: Instrumentation of the Homestake Underground Laboratory for Drawdown Measurements during Dewatering, *Proceedings*, SME Annual Meeting, Feb. 22-25, 2009, Denver, CO (2009).

Dobson, P.F., and R. Salve.: *Underground Reconnaissance and Environmental Monitoring Related to Geologic CO_2 Sequestration Studies at the DUSEL Facility, Homestake Mine, South Dakota*, LBNL-2858E, Lawrence Berkeley National Laboratory, Berkeley, CA (2009).

Fu, P., Johnson, S.M., and Carrigan, C.R.: An Explicitly Coupled Hydro-Geomechanical Model for Simulating Hydraulic Fracturing in Arbitrary Discrete Fracture Networks, *International Journal for Numerical and Analytical Methods in Geomechanics* (2013), 37 (14): 2278–2300..

Guo, B., Fu, P., Y. Hao, Peters, C.A., and Carrigan, C.R.: Thermal drawdown-induced flow channeling in a single fracture in EGS, *Geothermics*, 61, (2016), 46–62.

Hubbert, K. M., and Willis, D. G.: Mechanics of Hydraulic Fracturing, Transactions of the American Institute of Mining, Metallurgical, and Petroleum Engineers, (1957), 210(6), 153–163.

Mualem, Y.: New Model for Predicting Hydraulic Conductivity of Unsaturated Porous-Media, *Water Resources Research*, 12(3):513-522, doi:DOI 10.1029/WR012i003p00513 (1976).

Murdoch, L.C., L.N. Germanovich, H. Wang, T.C. Onstott, D. Elsworth, L. Stetler, and D. Boutt.: Hydrogeology of the vicinity of Homestake mine, South Dakota, USA, *Hydrogeology Journal*, 20:27-43, doi 10.1007/s10040-011-0773-7 (2012).

Knox H., et al.: Fracture and Flow Designs for the Collab / SIGMA-V Project, Geothermal Resources Council Transactions, (2017), 41.

Oldenburg, C.M., P.F. Dobson, Y. Wu, P.J. Cook, T.J. Kneafsey, S. Nakagawa, C. Ulrich, D.L. Siler, Y. Guglielmi, J. Ajo-Franklin, J. Rutqvist, T.M. Daley, J.T. Birkholzer, H. Wang, N.E. Lord, B.C. Haimson, H. Sone, P. Vigilante, W.M. Roggenthen, T.W. Doe, M.Y. Lee, M. Ingraham, H. Huang, E.D. Mattson, J. Zhou, T.J. Johnson, M.D. Zoback, J.P. Morris, J.A. White, P.A. Johnson, D. DD. Coblentz, and J. Heise.: *Intermediate-Scale Hydraulic Fracturing in a Deep Mine, kISMET Project Summary 2016*, LBNL-1006444, Lawrence Berkeley National Laboratory, Berkeley, CA (2016).

Roggenthen, W.M., and D.K. King,: Quick Review of T data for kISMET Area (5/19/17), *Unpublished EGS Collab Project Report*, Lawrence Berkeley National Laboratory, Berkeley, CA (2017).

Settgast, R.R., Fu, P., Walsh, S.D.C., White, J.A., Annavarapu, C., and Ryerson F. J.: A fully coupled method for massively parallel simulation of hydraulically driven fractures in 3-dimensions, Int. J. Numer. Anal. Methods Geomech., (2017), 41(5), 627–653.

Van Genuchten, MTA.: A closed-form equation for predicting the hydraulic conductivity of unsaturated soils, *Soil Science Society of America Journal*, 44:892-898, (1980).

Webb, S.W.: A simple extension of two-phase characteristic curves to include the dry region, *Water Resources Research*, 36(6):1425-1430, doi 10.1029/2000wr900057 (2000).

White, MD and M Oostrom.: *STOMP Subsurface Transport Over Multiple Phases, Version 4.0, User's Guide,* PNNL-15782 (2006).